Interaction of bone-dental implant with new ultra low modulus alloy using a numerical approach

Boris Piotrowski, A. A. Baptista, Etienne Patoor, P. Bravetti, André
Eberhardt, Pascal Laheurte

To cite this version :

Boris PIOTROWSKI, André BAPTISTA, Etienne PATOOR, Pierre BRAVETTI, André EBERHARDT, Pascal LAHEURTE - Interaction of bone-dental implant with new ultra low modulus alloy using a numerical approach - Materials Science and Engineering C - Vol. 38, p.151-160 - 2014

Interaction of bone-dental implant with new ultra low modulus alloy using a numerical approach

B.Piotrowski[1], A. A. Baptista[2], E.Patoor[1], P. Bravetti[2], A. Eberhardt[1], P. Laheurte[1*]

[1]*Laboratoire d'Etude des Microstructures et de Mécanique des Matériaux LEM3 (UMR CNRS 7239), ENSAM, Université de Lorraine, Ile de Saulcy, F-57045 Metz, France*

[2]*Faculty of Odontology, Nancy, France*

Abstract

Although mechanical stress is known as being a significant factor in bone remodeling, most implants are still made using materials that have a higher elastic stiffness than that of bones. Load transfer between the implant and the surrounding bones is much detrimental, and osteoporosis is often a consequence of such mechanical mismatch. The concept of mechanical biocompatibility has now been considered for more than a decade. However, it is limited by the choice of materials, mainly Ti-based alloys whose elastic properties are still too far from cortical bone. We have suggested using a bulk material in relation with the development of a new beta titanium-based alloy. Titanium is a much suitable biocompatible metal, and beta-titanium alloys such as metastable TiNb exhibit a very low apparent elastic modulus related to the presence of an orthorhombic martensite. The purpose of the present work has been to investigate the interaction that occurs between the dental implants and the cortical bone. 3D finite element models have been adopted to analyze the behaviour of the bone-implant system depending on the elastic properties of the implant, different types of implant geometry, friction force, and loading condition. The geometry of the bone has been adopted from a mandibular incisor and the surrounding bone. Occlusal static forces have been applied to the implants, and their effects on the bone-metal implant interface region have been assessed and

compared with a cortical bone/ bone implant configuration. This work has shown that the low modulus implant induces a stress distribution closer to the actual physiological phenomenon, together with a better stress jump along the bone implant interface, regardless of the implant design.

1. Introduction

Over the last few decades, considerable progress in dental implantology has been made, with success rates exceeding 95% [1]. Implant stability is commonly considered as playing a major role in a successful osseointegration. Obtaining post-operative osseointegration is necessary in order to establish a solid and durable connection between the implant and the osseous structure. In agreement with the Wolff law, a process of osseous remodelling adapted to the stress level occurs after implantation [2-4]. This process is controlled by mechanical loads. When the occlusal forces induced on the bone exceed a physiological level, bone resorption can occur, with possible failure [5]. More importantly, the long-term performance of an implant is known to be strongly dependent on the bone tissue interaction [6]. The strain state which takes place at the interface between the bone and implant controls the bone tissue remodelling mechanisms [7]. Bone resorption is associated with a low strain state, and bone necrosis occurs when strain exceeds the maximum level.

Evaluation of the risk requires a comprehension of the load transfer along the bone-dental implant interface. This allows for 1) a decrease in the risk of failure of the bone / implant interface during stress transfer, and 2) a reduction of the appearance of relative micro-motions, induced by the stress jump between the implant and surrounding bones, which is responsible for a loss of mechanical stability [5].

In accordance with Wolff's law, the loading stress limits of the bone are determined by physiological factors. Load transfer between an implant and the surrounding bone has recently been intensively studied using Finite Element Modelling [8]. Several parameters related to the implant have to be considered, such as geometry, loading, the interaction between the implant and the cortical bone, and material properties.

A considerable number of experimental and numerical studies have been carried out to understand the mechanism of the load transfer from the implants to the bones [9-16]. A geometric influence has been demonstrated. The thread shape likely plays a major role in the load transfer from the dental implant to the surrounding bones. However, in these studies, the parameter that is most commonly optimized is the implant shape, and the influence of its elastic properties is less often considered [8]. The development and optimization of implants must then involve geometrical, mechanical, and material considerations [17] to adjust the stress state to admissible physiological values that are as close as possible to the conditions of a natural tooth [18].

This mechanical regime is largely dependent on Young's modulus of the implant; but most of the implants are still made of materials that have a higher elastic stiffness - steel, CP titanium and TA6V - than that of the cortical bone. Due to this difference in stiffness, the load transfer between the implant and the surrounding bones is much detrimental, and stress distribution in the bones is far from the physiological case: Young's modulus should be as close as possible to that of the host bone to achieve a homogeneous load transfer between the implant and the bone. This becomes an important issue for biomaterials selection, and the concept of mechanical biocompatibility is rather new [19, 20].

Three kinds of solutions have been developed to achieve mechanical compatibility. The first

considers porous materials and adjusts porosity to match the elastic modulus of human bone [21, 22]; the second relates to the utilization of HAP [23, 24]; the third focuses on bulk materials that present low intrinsic elastic constants. The third approach was first introduced in Japan at the beginning of the 2000s [25].

In this paper, we propose to study the effect of a low modulus bulk implant on load transfer into surrounding bones, as well as the stress jump between them. The adopted material is a bulk material, and consists of a new beta titanium-based alloy with ultra low modulus and high ultimate tensile strength, which is studied within the framework of the French National Research Agency through the Functional Materials and Innovative Processes Program, Grant No ANR-08MAPR-0017. An « ultra low modulus » refers to Young's modulus close to that of bone, and differs from the elasticity modulus usually encountered in beta titanium alloys (around 60-70 GPa). Both high strength and a low Young's modulus are required for dental applications. Depending on the type of thermomechanical treatment they have undergone, TiNb alloys, with a composition ranging from Ti-23Nb to Ti-26Nb, can have varying Young's modulus. Recently, we have demonstrated that severe cold rolling deformation followed by flash aging treatment on TiNb and TiNbZr, in order to produce ultra fine grains and/or omega phase, is more effective to improve strength [26-30]. High ultimate tensile strength (800 MPa), and low modulus (30 GPa) are obtained by nanostructuration process, as illustrated in Fig. 1. These characteristics are due to the stress-induced martensitic transformation and its reverse transformation, accompanied by the formation of ultra-fine beta grain by flash treatment at 873K, or omega precipitation by flash treatment at 573K. Moreover, these alloys contain non-toxic alloying elements, such as Nb, Ta, Mo and Zr, and exhibit superior biocompatibility [31-33] and lower toxicity than that of TA6V alloy [34].

A Finite Element (FE) model taking into account stress distribution into the implant and the bones under a static loading is investigated. The model considers one implant inserted into a mandibular cortical and trabecular bones. Several cases are studied with various implant elastic properties, considering a Young's modulus of 210, 110 and 30 GPa. A geometric reference model is established and is similarly used for all simulations, while the elastic modulus of the implant is modified (15 GPa). The maximal and minimal stresses obtained in the bones surrounding the implant are compared with the results of the reference FE simulation, where the implant has a Young's modulus close to dentine. Moreover, the stress jump at the interface between the implant and the mandible is studied. The influence of the geometry of the contact surface and the loading force are also studied. The purpose of this work is to show the influence of a low modulus implant on the interaction of the bone implant interface, regardless of the implant design. In this study, we highlight the fact that the elasticity modulus itself has a strong impact on load transfer (stress) between the implant and the bone during loading. We particularly focus on two strategic areas which are well known as sources of mechanical stability problems: the top of the implant-cortical bone interface, with, for example, saucerization [35] due to local overload-induced microfracture [36] or insufficient stress to maintain implant stability [37], and the bottom of the implant-cortical bone interface, which is usually overstrained due to the conical implant shape. These two areas are respectively named TOP and BOTTOM.

2. Finite Element Model

In this study, the improvement of implant mechanical stability is investigated via a FE model and the implant elastic properties. The studied model represents one elastic implant inserted in a mandible bone, and is composed of two parts: implant and bones, cortical and trabecular. The aim of this study is not to predict the exact stress magnitude in the considered parts, but

to evaluate the influence of the implant elastic properties on stress shielding. Thus, three hypotheses have been adopted, such as the homogeneous isotropic constitutive law of bone and implant. Moreover, among marketed implants, quite a large number of implants with complex shapes are to be found, the geometrical features of which affect their overall behavior. To avoid parasitic effects, two simplified shapes have been considered for implants. Similarly, as the bone shapes and specific dimensions are related to several physiological parameters the study of which is beyond the scope of this work, the mandible shape has been modelled with a simplified shape.

2.1 Implant material characteristics

In the present study, four Young's Moduli have been considered and listed in Table 1. For the TiNb ultra low modulus alloy, a Young's modulus of 30 GPa has been considered. In current implantology, TA6V implant is adopted with a Young's modulus around 110 GPa, close to CP - Ti. Then, steel implant [38] as well as an implant with an elasticity modulus as close as possible to that of dentine (15 GPa) have been considered. In the case of dentine, stress distribution has been assumed to be optimal and identical to the physiological one. It has been used as a reference to which the other configurations have been compared. This physiological case will subsequently be referred to as R_C (Reference Case). In each studied case, elastic behavior is assumed to be isotropic and Poisson's ratio is equal to 0.3.

2.2 Bone material characteristics

The mandible is composed of a trabecular bone surrounded by a layer of cortical bone. The thickness of this layer, and the density, as well as the mechanical properties of each kind of bones are sensitive to several parameters such as the age and sex of the patient. Indeed, the thickness of the cortical bone is not the same everywhere in the mandible. It has been shown that the elastic properties of bones are anisotropic [39-40]. However, elasticity is often

6

considered as isotropic in the FE model of implants in the mandible [41-44], and it has been shown that the impact of anisotropy on the stress state into a bone is limited, with a maximal difference lower than 10 % [45]. Moreover, bones are assumed to be homogeneous with a linear elastic behaviour. Further investigations will take into account the anisotropic character of bone elasticity.

As the Young's modulus of the cortical and the trabecular bones is difficult to determine experimentally, adapted values for cortical and trabecular bones have been considered (15 GPa and 1 GPa, respectively) [46].

2.3 Creation of the 3D implant-mandible models

Altough an axisymmetric model could be used to represent the implant shape [47], especially in a smooth case, the boundary conditions and the shape of the mandible are not axisymmetric. A 2D model in plane strain hypothesis could be used to model the mandible [48-49], but in this case the modelled implant shape would be far from the real one. Two 3D geometrical models have been considered to study the load transfer between the implant and the mandible, as illustrated in Fig. 2. The aim is to highlight the benefit of a low modulus, and the geometrical features of the forefront TA6V implants have not been considered. The geometrical models have been simplified to reduce the impact of geometric features. In the first one, the implant is smooth (S-MODEL), whereas in the second, it is threaded (T-MODEL). The geometrical model of the implant is based on a commercial implant which has been slightly modified and simplified. It is composed of the cortical bone, in white in Fig. 2, containing the trabecular bone, not represented on the Figure. The geometrical model of the mandible is represented in Fig. 3. In both models, the cortical and trabecular bones have the same dimensions. The thickness of the cortical bone is assumed to be constant, and equal to 2 mm [44]. In the S-MODEL, the implant is composed of a conical part and a cylindrical part. The conical part has a diameter reduced from 4.5 to 3.5 mm on a length of 2 mm, and the

cylindrical part has a diameter of 3.5 mm on a length of 15 mm. In the T-MODEL, the implant dimensions are based on a smooth one, 4 picos are added in the conical part, and the cylindrical part is threaded. The bones are threaded in order to allow for the insertion of alloy implant with contact between different parts. The implant and bones have been designed with the CAD Catia_V5R16 software (Dassault Systèmes).

2.4 Characteristics of the simulations

The complete models have been imported into the V6.11-2 Abaqus (Dassault Systèmes) finite element calculation software. A general static step has been considered in order to load the implants. The smooth implant has been meshed with C3D20 quadratic hexahedron continuous and isoparametric finite elements with a minimum size of 0.25 mm, as illustrated in Fig. 4. The threaded implant has been meshed with C3D4 linear tetrahedron continuous and isoparametric finite elements with a minimum size of 0.125 mm, and with C3D8 linear hexahedron continuous and isoparametric elements. C3D4 elements are required to accurately model the threads, whereas C3D8 elements have been used to mesh the upper part of the implant. Cortical and trabecular bones have been modelled with C3D20 quadratic hexahedron continuous and isoparametric finite elements. The critical element length depends on the implant geometry, which is defined as the master surface. The same order of element size in the contact surface between the implant and bones has been adopted in order to limit computation time and ensure accurate results. In the region with no major stress gradient, larger elements have been adopted. The mesh has been handled with the advancing front mesh method available among the Abaqus mesh tools, and several simulations have been conducted to ensure that the element size has no influence on the solution. In the smooth case, 242,000 degrees of freedom have been required to mesh the implant, 1,530,900 for the cortical bone and 187,820 for the trabecular one. In the threaded case, 543,116 elements have been required to mesh the implant, 24,640,780 for the cortical bone and 6,272,640 for the trabecular one.

The substantial number of elements required to model the threaded implant is significantly higher than that of the smooth implant. This is due to the difficulty of taking the threads into account with at least two elements in their thickness. The meshed parts of the S-MODEL and T-MODEL are represented in Fig. 4. The specified boundary conditions are as follows, illustrated in Fig. 5:

– The two plane surfaces of the cortical and trabecular bones have been encastred;

– The displacement degrees of freedom at the interface between the cortical and the trabecular bones are tied;

– Contact with friction between the implant and the bones (cortical and trabecular) is assumed, with a friction coefficient of 0.3 [8];

Concerning the smooth configuration, an axial load of 160 N, currently adopted to simulate a classical mastication load [45], is applied with a pressure of 10 MPa on a surface of 16 mm². In the threaded model, two loaded cases are considered: axial loads of 160 and 300 N, respectively, applied with a pressure of 10 and 18.75 MPa on 16 mm² surfaces. The cases with 300 N are studied to model unusual loadings such as bruxism or the loss of contact sensitivity. In this study, axial loads only are considered, to avoid an additional parameter influencing the highlighted material effect.

Simulations have been performed on a Dell PowerEdgeR410 (2x Intel_Xeon_quadcore 2.93 GHz, 24 GBRAM). The average calculation time was about four hours for each model.

3. Results and discussion

This section deals with the stress fields in the implants and in the bones under the applied loads in the studied configurations. The stress fields on the peri-implant cortical bone are evaluated for a static loading. As explained earlier, we focused on two different results. The first is the stress distribution in bones around the implant/mandible interface, and the second

is the stress jump between the implants and the cortical bones. Results are presented in two configurations: the S-MODEL with an axial load of 160 N, and the T-MODEL with axial loads of 160 and 300 N.

Results are represented along the cortical bone/implant interface. In the S-MODEL, 14 elements are in contact, 7 on each side. In the T-MODEL, 32 elements are in contact, 16 on each side. Fig. 6 illustrates the numbering of the represented contact elements.

3.1 S-MODEL with axial load of 160 N

Fig. 7 represents the Von Mises stress field in the cortical bone for Young's modulus of the four implants. Results are given in a 2D plane, and it can be considered that there is an axisymmetry in the stress values. The area at the top of the implant, denoted 1, is thought to be the one from which infections appear. It can be seen that in the R_C, the stress field in this area is between 7 and 13 MPa. This value is well below that found in the cases of steel and TA6V, the materials mainly used for dental implants, with stress fields ranging between 20 and 27 MPa. It can be seen that in the TiNb case, the maximal stress in the TOP area is reduced by 2 compared with the TA6V case, and the difference from the R_C is around 5 MPa. In order to present the results with the same representative isocolours, the maximal stress is considered to be 80 MPa. Above this value, the stress is presented in grey. At the bottom of the cortical bone, the BOTTOM area, it can be seen that the grey area is present in each case. However, the maximal stress values obtained in steel, TA6V, TiNb and R_C are 140, 139, 127 and 122 MPa, respectively. Thus, the implant with low modulus again creates stresses closer to the R_C.

Fig. 8 represents the Von Mises stress difference, inside the cortical bone along the bone/implant interface, between the cases with steel, TA6V and TiNb implants, and the R_C. It illustrates the gap of the stress inside the cortical bone due to the implant during loading. It

can be seen that for the seven pairs of elements, the stress inside the cortical bone with TiNb implant is closer to the physiological stress than the stress obtained with the TA6V implant. In the TOP area, in which the loss of mechanical stability with the TA6V implants begins, the difference in stress is decreased by 65 %. In the inferior part of the implant in contact with the cortical bone, where the stress magnitude is the greatest, the stress difference between the R_C, TA6V, and TiNb cases is about 50 %. These results emphasize the interest of low Young's modulus implant. An interesting result is that the evolution of the difference in stress is not linear with Young's modulus of the implant. For example, for pair 1, the stress difference between the R_C and the steel implant is about 10 MPa, that between the R_C and the TA6V implant is 8.4 MPa, and that between the R_C and the TiNb implant is 2.9 MPa. In pairs 2 and 3, the influence of the implant alloy is limited. Indeed, in Figure 7 it can be seen that the influence is in the top and bottom areas of the contact region. In pairs 2 and 3, the difference between alloys is less than 0.2 MPa. The stress difference is greater for TA6V implants (1.2 and -1.4 respectively) than for steel implants (0.8 and 1.1) and for TiNb implants (0.95 and -1 MPa). The stress distribution inside the cortical bone is strongly related to the stress inside the implant. In the case of steel, the high implant rigidity induces considerable stress at the top of the implant, and substantial stress transfer between the implant and the cortical bone in the upper part of the interface. In comparison, for TiNb, the stress has better propagation inside the implant, and the stress transfer at pair 3 is equivalent to the steel and the TA6V cases. Pair 3 is the only one for which the stress induced by the implant is lower than physiological stress. Between pairs 1 and 3, there are some points where the difference between physiological stress and that induced by the implant is equal to zero. These points are not collocated. This result can be seen in Fig. 9, which represents the Von Mises stress field in both the implant and the cortical bone under a load of 160 N.

Fig. 10 shows the Von Mises stress jump between the cortical bones and the implant, and

highlights the differences between the steel, TA6V and TiNb cases, and the R_C. It illustrates the gap in stress jump, due to the implant, between the cortical bone and the implant. In the upper part, the stress jump difference in the R_C between the TA6V and TiNb cases is considerable. A 62 % decrease is observed for the TiNb implant compared with the classical TA6V implant. This difference is about 43 % in the BOTTOM area where the stress is greater. Nevertheless, it can be seen that the stress jump difference with the R_C is 25 % greater with the TiNb implant than with the TA6V implant for pair 6. This is the only pair for which the TA6V implant is closer to the R_C, but this area is not known as the one which induces mechanical stability problems. Generally, it can be seen that the stress jump is greater when Young's modulus of an implant is high, and that this evolution is not linear. For example, in the upper area, the stress jump difference is about 15 % between the steel and the TA6V cases, whereas Young's modulus difference is 50 %, and the stress jump difference is about 70 % between the steel and the TiNb cases, whereas Young's modulus difference is 30 %.

3.2 T-MODEL with axial loads of 160 and 300 N

In this section, two T-MODEL cases are studied with applied loads of 160 and 300 N. The influence of the implant shape will be discussed in the next section. Fig. 11 represents the stress field in both the implants and the cortical bones. On the left (A, B, C and D), the results are obtained with a load of 160 N, whereas those on the right (E, F, G and H) are obtained with 300 N. It can be seen that, with a threaded implant shape, the TiNb implant induces a stress distribution inside the cortical bone close to the R_C. The difference is greater with the TA6V implant, and it can be seen that in specific areas the differences reach up to 6 MPa. Fig. 12 represents the stress gap between the implanted cases and the physiological one for the three considered alloys. For a load of 160 N, the stress distribution in the cortical bone with a TiNb implant is almost always significantly closer to the R_C compared with the TA6V implant. Indeed, at the top of the implant, the stress induced by the load on the TiNb implant

is almost the same for pairs 1, 2, 3 and 4, whereas a stress diminution is found for more rigid implants. According to Wolff's law, a stress lower than that physiologically required could induce bone resorption and implant failure. However, in this situation, the amplitude of stress diminution is low. For pairs at the middle and the bottom of the implant/cortical bone contact, the predicted stress for the TiNb implant never exceeds 3 MPa for the predicted physiological stress, whereas it exceeds 7 MPa for the steel implant for pairs 11 to 15, and is greater than 6 MPa in the TA6V implants for pairs 12 to 15. It can be seen that the TiNb implant gives better results in the critical areas where problems are encountered (TOP and BOTTOM areas). The situation is the same when the load is 300N. For the TiNb implant, the stress distribution induced by the material characteristics in the cortical bones is closer to the R_C compared with those of the more rigid implants. However, it can be seen that the benefits of a low modulus are smaller. This is explained by the stress distribution inside the implant. As can be seen in Fig. 13, the stress field and therefore the strain energy in the bottom part of the implant surrounded by the cancellous bone is much greater when the applied load is 300 N. For 160 N, the strain energy is mainly dissipated into the cortical bone (33 MPa) via the implant/bone interface and the stress field in the BOTTOM part of the implant does not exceed 10 MPa. For 300 N, the maximal stress increase in the cortical bone is less than 10 %, whereas the maximal stress increase in the bottom part of the implant is about 65 %. The stress inside the cortical bone is closer to the R_C at 300 N, regardless of the implant material.

Fig. 14 illustrates the stress jump gap between the R_C and the implant case, for a load of 160 N (top) and 300 N (bottom). It can be seen that for the 160 N load, the stress jump in the critical areas for the TiNb implant is close to the physiological stress jump (pairs 1, 2 and 3 at the top and pairs 15 and 16 at the bottom), unlike other implants made of steel and TA6V alloys. The trend is the same for the 300 N load at the bottom part of the implant/cortical bone contact area. The benefit is less significant for the top area: in pairs 1 and 2. The three kinds

of implants induce the same stress jump, and the gap with the R_C is not really affected. However, pairs 3 to 6 are significantly close to the R_C for the TiNb implant.

3.3 Shape effect

It can be seen that the implant shape plays an important role in the maximal stress in the cortical bone. Fig. 15 shows the evolution of stress in the cortical bone neighbouring the contact surface for the two TiNb implants loaded at 160 N. It can be seen that, with a threaded shape, the stress is better distributed. In the S-MODEL, the stress in the cortical bone exhibits a steady increase up to 62 MPa. In the T-MODEL, four stages of stress are clearly identified. This result is highlighted for steel, TA6V and TiNb implants. In the TOP area, close to the surface where pressure is applied, the stress field is not affected by the implant shape. In the BOTTOM area, the stress field is 50 % higher in the S-MODEL than in the T-MODEL.

4. Conclusion

a) The stress distribution is much closer to the reference situation with a TiNb implant than with TA6V and steel implants. This result is obtained whatever the shape of the implant and the applied load. The stress gap is significantly reduced, which induces a decrease in the stress shielding.

b) The stress jump at the interface between the cortical bone and implant decreased significantly with the use of a low Young's modulus implant, for each studied configuration. This reduces the micro-motions in the cortical bone-implant interface.

c) The influence of the low modulus on stress distribution is not proportional to the applied load.

d) The stress distribution is also related to the shape of the implant, as the shape amplifies or reduces the benefit of the low modulus implant. The threads allow stress in the bone to be staged and they thus limit the maximum stress in the lower part of the cortical bone-implant

interface. The reduction of the stress shielding requires both an adapted shape and a low modulus material. Beyond biocompatibility, we have demonstrated that TiNb material can achieve mechanical compatibility.

References

[1] D. Buser, S.F. Janner, J.G. Wittneben, U. Brägger, C.A.Ramseier, G.E.Salvi, Clin. Implant. Dent. R. 14 (2012) 839-890.

[2] H. Weinans, R. Huiskes, H.J. Grootenboer, J. Biomech. 25 (1992) 1425-1441.

[3] C. Jacobs, J. Simo, G. Beaupré, D. Carter, J. Biomech. 30 (1997) 603-613.

[4] S.C. Cowin, Calcified. Tissue Int. 36 (1994) S98-S103.

[5] R. De Santis, F. Mollica, F. Zarone, L. Ambrosio, L. Nicolais, Acta Biomater. 3 (2007) 121-126.

[6] D.A. Puleo, A. Nanci, Biomaterials 20 (1999) 2311-2321.

[7] M. Doblaré, J.M. Garcia, J. Biomech. 34 (2001) 1157-1170.

[8] H. Guan, R. Van Staden, Y.C. Loo, N.W. Johnson, S. Ivanovski, N. Meredith, Int. J. Oral Max. Impl. 24 (2009) 866-876.

[9] A.N. Natali, P.G. Pavan, A.L. Ruggero, Clin. Oral Impl. Res. 17 (2006) 67-74.

[10] S.J. Hoshaw, J.B. Brunski, G.V.B. Coebran, Int. J. Oral Max. Impl. 9 (1994) 345-360.

[11] A.N. Natali, The simulation of load bearing capacity of dental implants, in: J. Vander Slote (Eds.), Computer Technology in Biomaterials Science and Engineering, John Wiley & Sons, New York 1999, pp. 132-148.

[12] A.N. Natali, P.G. Pavan, Numerical approach to dental biomechanics, in: A. N. Natali (Eds.), Dental Biomechanics, Taylor & Francis, London, 2003, pp. 211-239.

[13] H. Guan, R. Van Staden, N.W. Johnson, Y. Chaye, Finite Elem. Anal. Des. 47 (2011) 886-897.

[14] L. Baggi, I. Cappelloni, F. Maceri, G. Vairo, Simul. Model. Pract. Th. 16 (2008) 971-987.

[15] G. Limbert, C. Van Lierde, O. Luiza Muraru, X. Frank Walboomers, M. Frank, S. Hansson, J. Middleton, S. Jaecques, J. Biomech. 43 (2010) 1251-1261.

[16] S. Faegh, S. Muftu, J. Biomech. 43 (2010) 1761-1770.

[17] E. Castro Ferreira, S. Corbella, L.C. Zanatta, S. Taschieri, M. Del Fabbro, S.A. Gehrke, Minerva Stomatol. 61-6 (2012) 262-271.

[18] L. Girod, V. Berry-Kromer, T. Ben-Zineb, A. Eberhardt, E. Patoor, B. Prandi, IJIDEM 4-3 (2010) 157-167.

[19] N. Sumitomo, K. Noritake, T. Hattori, K. Morikawa, S. Niwa, K. Sato, M. Niinomi, J. Mat. Sci.: Materials in Medicine 19-4 (2008) 1581-1586.

[20] M. Niinomi, M.M. Nakai, Int. J. Biomater. 2011 (2011) 1-10.

[21] E.D. Spoerke, N.G. Murray, L.C. Brinson, D.C. Dunand, S.I. Stupp, Acta Biomater. 1 (2005) 523-533.

[22] J. Chen, C. Rungsiyakull, W. Li, Y. Chen, M. Swain, Q. Li, J. Mech. Behav. Biomed. Mater. 20(2013) 387-397.

[23] H.S Hedia, N.A. Mahmoud, Biomed. Mater. Eng. 14 (2004) 133-143.

[24] D. Lin, Q. Li, M.W. Swain, Compos Part B-Eng. 40 (2009) 668-675.

[25] M. Niinomi, Biomaterials 24 (2003) 2673-2683.

[26] P. Laheurte, F. Prima, T. Gloriant, M. Wary, E. Patoor, J. Mech. Behav. Biomed. Mater. 3-8 (2010) 565-573.

[27] F. Sun, S. Nowak, T. Gloriant, P. Laheurte, A. Eberhardt, F. Prima, Scripta Mater. 63-11 (2010) 1053-1056.

[28] F. Sun, Y.L. Hao, S. Nowak, T. Gloriant, P. Laheurte, F. Prima, J. Mech. Behav. Biomed. Mater. 4-8 (2011) 1864-1872.

[29] W. Elmay, E. Patoor, B. Bolle, T. Gloriant, F. Prima, A. Eberhardt, P. Laheurte, Comput. Methods Biomec. 14-S1 (2011) 119-120.

[30] A. Ramarolahy, P. Castany, F. Prima, P. Laheurte, T. Gloriant, J. Mech. Behav. Biomed. Mater. 9 (2012) 83-90.

[31] A. Najdahmadi, A. Zarei-Hanzaki, E. Farghadani, Mater. Design 54 (2014) 786-791.

[32] M.A.H. Gepreel, M. Niinomi, J. Mech. Behav. Biomed. Mater. 20 (2013) 407-415.

[33] K.Y. Xie, Y. Wang, Y. Zhao, L. Chang, G. Wang, Z. Chen, Y. Cao, X. Liao, E.J. Lavernia, R.Z. Valiev, B. Sarrafpour, H. Zoellner, S.P. Ringer, Mater. Sci. Eng. C 33 (2013) 3530-3536.

[34] D. Kuroda, M. Niinomi, M. Morinaga, Y. Kato, T. Yashiro, Mater. Sci. Eng. A 243 (1998) 244-249.

[35] A. Consolaro, R. Savi de Carvalho, C.E. Francischone Jr, M.F.M.O. Consolaro, C.E.

Francischone, Dental Press J. Orthod. 15-3 (2010) 19-30.

[36] W.E. Roberts, L.P. Garetto, R.A. De Castron, J. Indiana Dent. Assoc. 68 (1989) 19-24.

[37] H. Vaillancourt, R.M. Pilliar, D. McCammond, J. Appl. Biomater. 6 (1995) 267-282.

[38] T. Albrektsson, G. Zarb, P. Worthington, A.R. Eriksson, Int. J. Oral Max. Impl. 1-1 (1986) 11-25.

[39] P. I. Brånemark, U. Lekholm, G.A. Zarb, T. Albrektsson, Tissue-Integrated Prostheses. Quintessence Publishing, Chicago, 1985.

[40] A.M. O'Mahony, J.L. Williams, P. Spencer, Clin. Oral Implan. Res. 12 (2001) 648-657.

[41] J.S. Feine, G.E. Carlsson, M.A. Awad, A. Chehade, W.J. Duncan, S. Gizani, T. Head, J.P. Lund, M. MacEntee, R. Mericske-Stern, P. Mojon, J. Morais, I. Naert, A.G. Payne, J. Penrod, G.T. Stoker, A. Tawse-Smith, T.D. Taylor, J.M. Thomason, W.M. Thomson, D. Wismeijer, Int. J. Oral Max. Impl. 17-4 (2002) 601-602.

[42] M. Oetterli, P. Kiener, R. Mericske-Stern, Int. J. Prosthodont. 14 (2001) 536-542.

[43] B. Engquist, P. Astrand, B. Anzen, S. Dahlgren, E. Engquist, H. Feldmann, U. Karlsson, P.G. Nord, S. Sahlholm, P. Svardstrom, Clin. Implant. Dent. R. 7 (2005) 95-104.

[44] S.M. Heckmann, W. Winter, M. Meyer, H.P. Weber, M.G. Wichman, Clin. Oral Implan. Res. 12 (2001) 617-623.

[45] M. Daas, Contribution à l'étude du comportement biomécanique de l'environnement d'un implant dentaire, PhD thesis, Paul Verlaine University, Metz, France, 2008.

[46] G. Odin, C. Savoldelli, P.O. Bouchard, Y. Tillier, Med. Eng. Phys., 32-6 (2010) 630-637.

[47] J.R. Klepaczko, T. Lodygowski, Advances in Constitutive Relations Applied in Computer Codes, ed. Springer, Vienna, 2009.

[48] J.P. Geng, W. Xu, K.B.C. Tan, G.R. Liu, J. Oral Implant. 30-4 (2004) 223-233.

[49] N.L. Grundling, C.H. Jooste, E. Terblanche, Int. J. Oral Max. Impl. 10 (1995) 51-57.

.
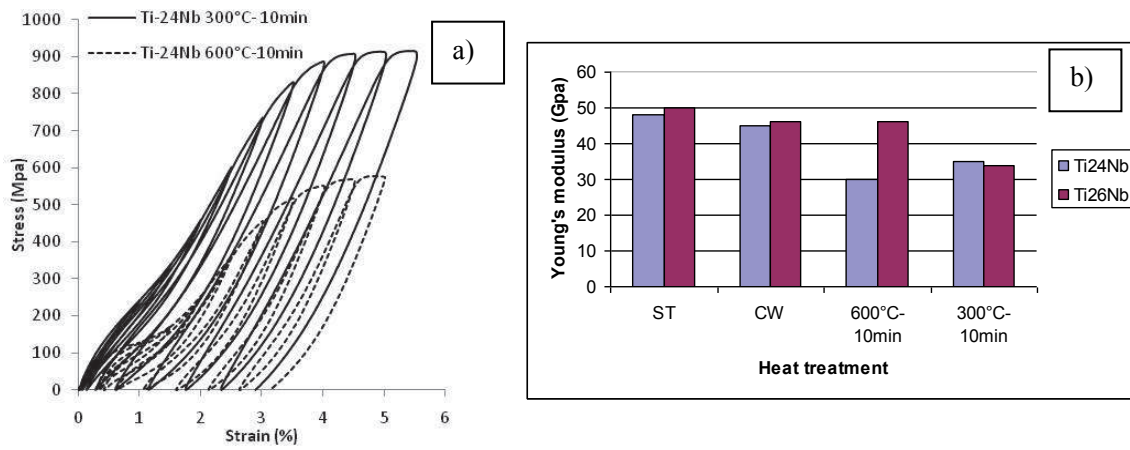
Fig. 1 - (a) Effect of cyclic deformation on stress-strain curves of CWA873 and CWA573 specimens for Ti-24Nb and (b) Young's modulus for ST, CW, CWA873 and CWA573 specimen Ti-24Nb and Ti-26Nb alloys [29]

Table 1 - Four different values of Young's modulus considered for the implant:

Alloys	Young's modulus (GPa)
Steel	210 GPa
CP Titanium	110 GPa
TiNb low modulus	30 GPa
Dentine – Reference case R_C	15 GPa
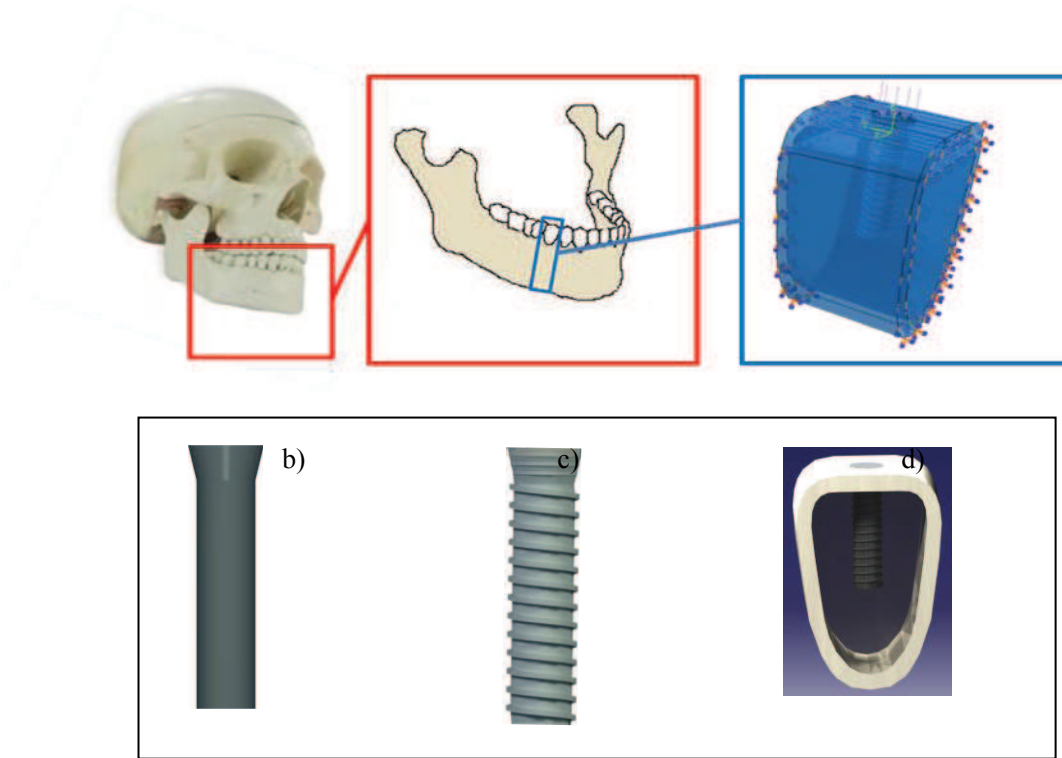
Fig. 2 - Representation of considered parts in the FE model (a); S-MODEL (b); T-MODEL (c); and set thread implant/mandible (d, only cortical bone is represented).
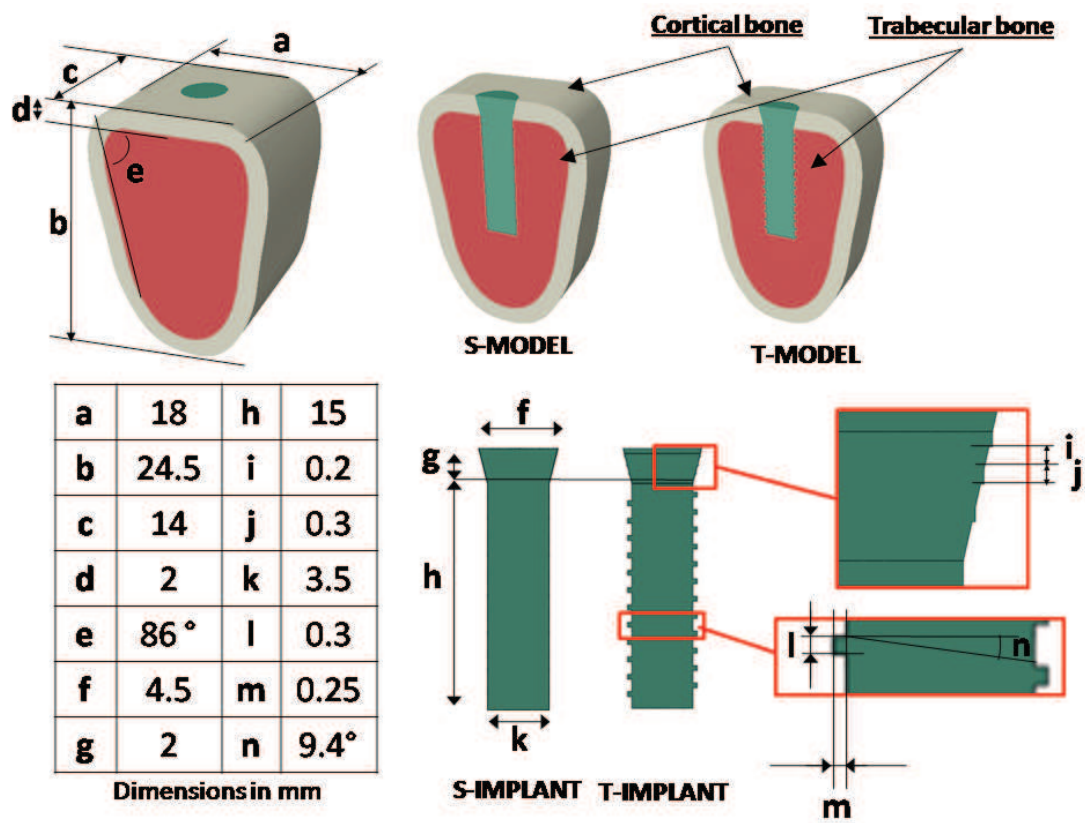
Fig. 3 - Geometric parameter values of considered model
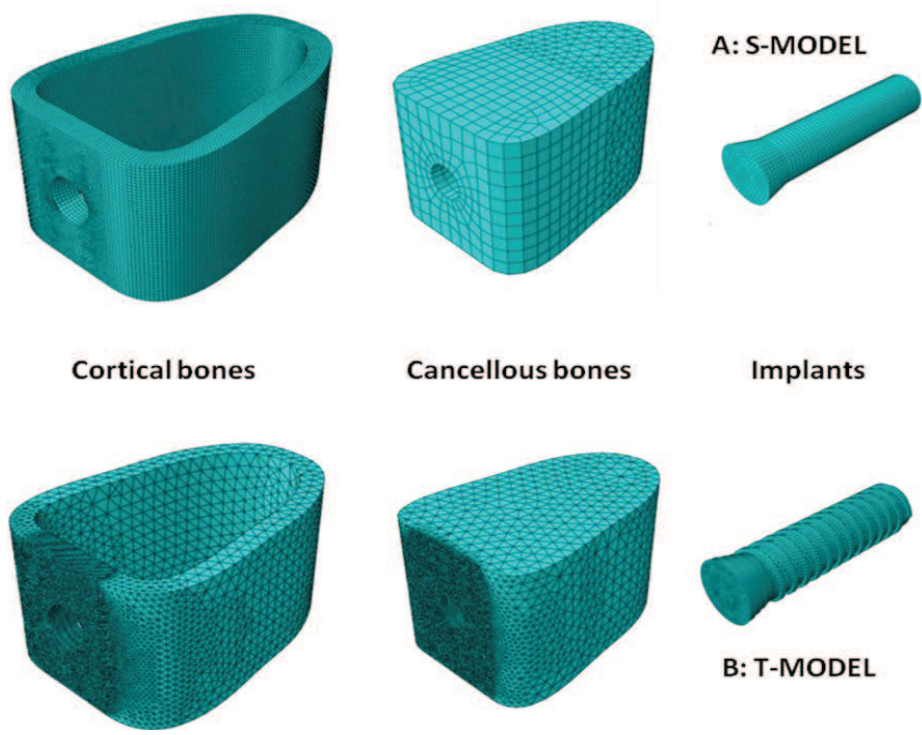
Fig. 4 - Mesh representation of cortical bone (left), trabecular bone (middle) and implant (right) in the threaded case. A: S-MODEL, B: T-MODEL
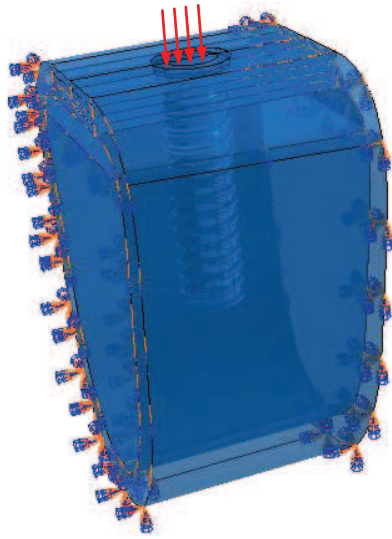
**Fig. 5 -** Boundary conditions and loads applied on the adopted model
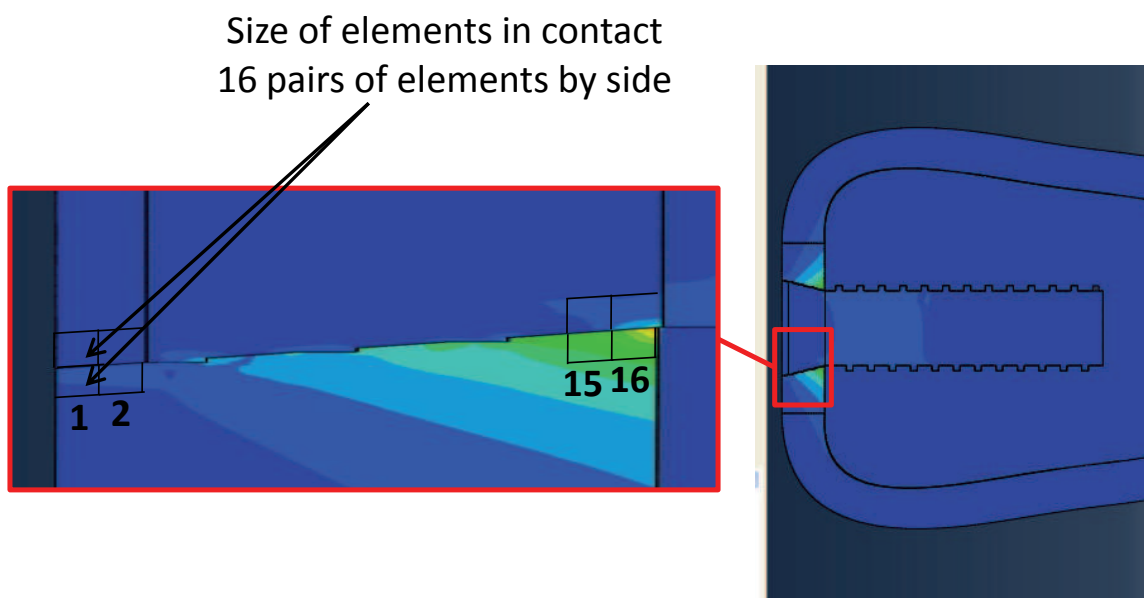
Fig. 6 - Numbering of the contact pair elements between the cortical bones and the implants - Example of the T-MODEL case with 32 elements in the contact area in the 2D representation (14 elements in the smooth case)
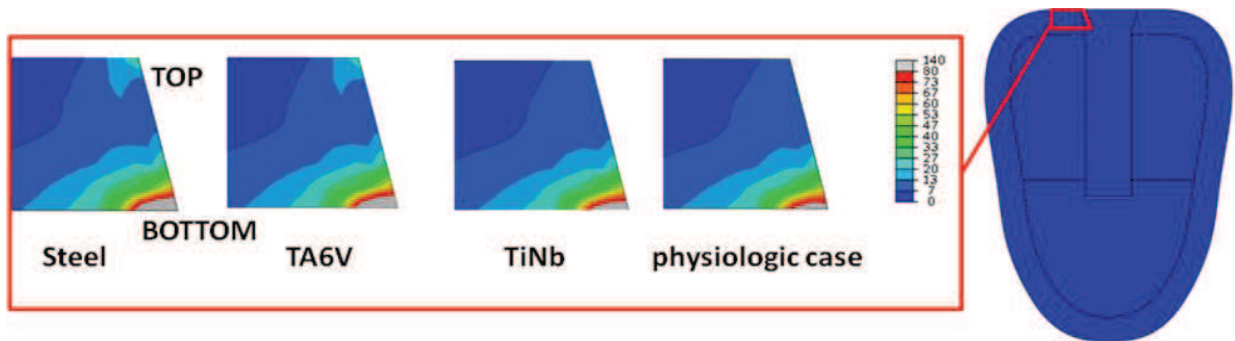
Fig. 7 - Representation of Von Mises stress field in the cortical bone for an axial load of 160 N in the S-MODEL. Four implants with different Young's moduli are considered: a) Steel; b) TA6V; c) TiNb; d) R_C
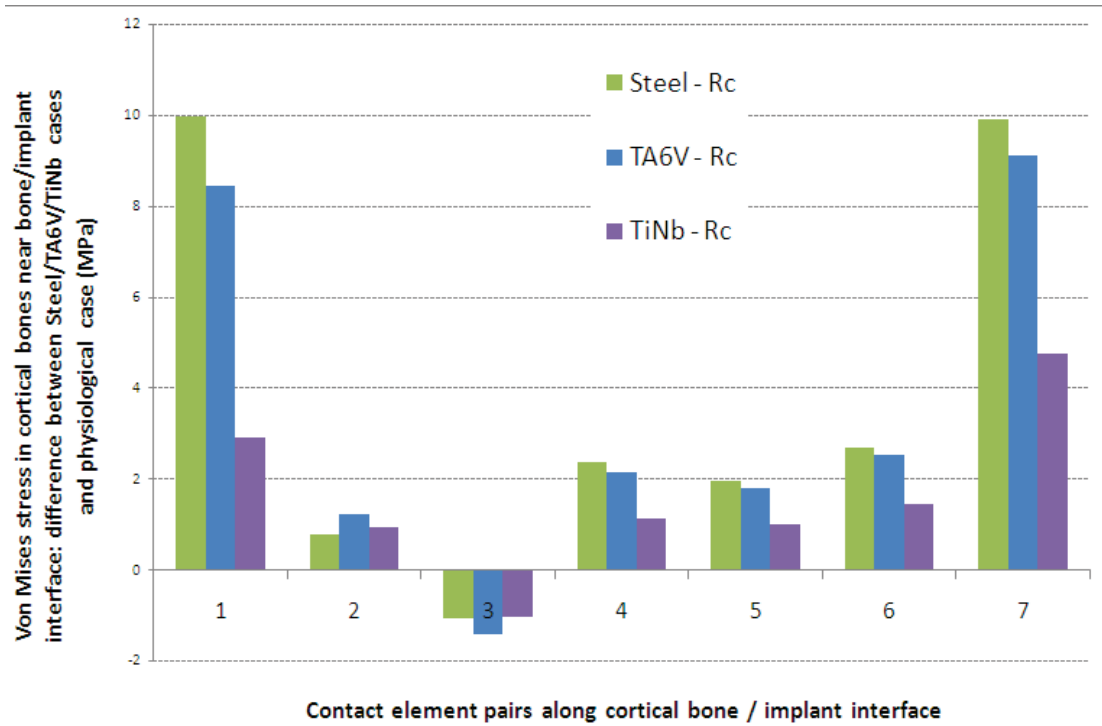
Fig. 8 - Representation of Von Mises stress in the cortical bone along the bone/implant contact surface for an axial load of 160 N in the S-MODEL. Three Young's moduli of implant are considered: Steel - R_C ; TA6V - R_C ; TiNb - R_C
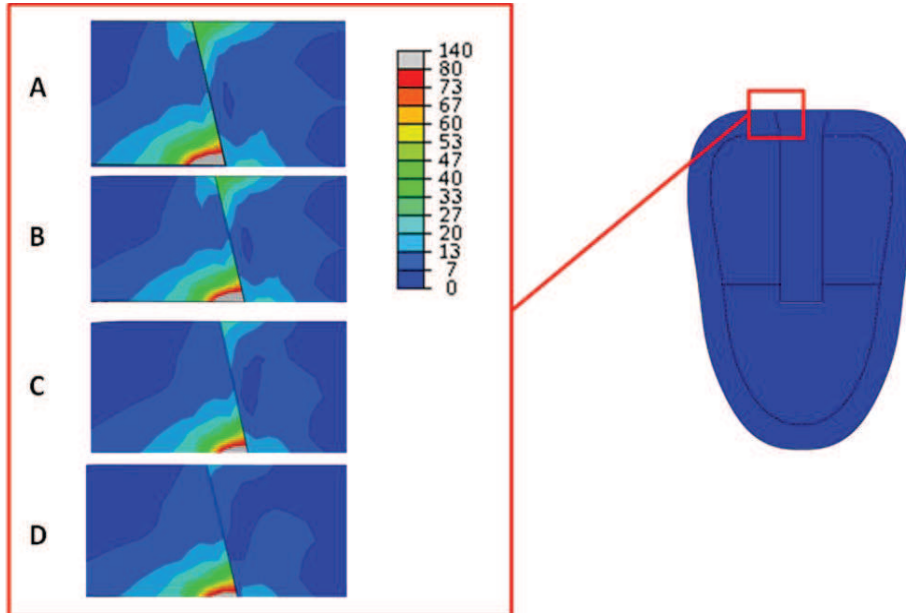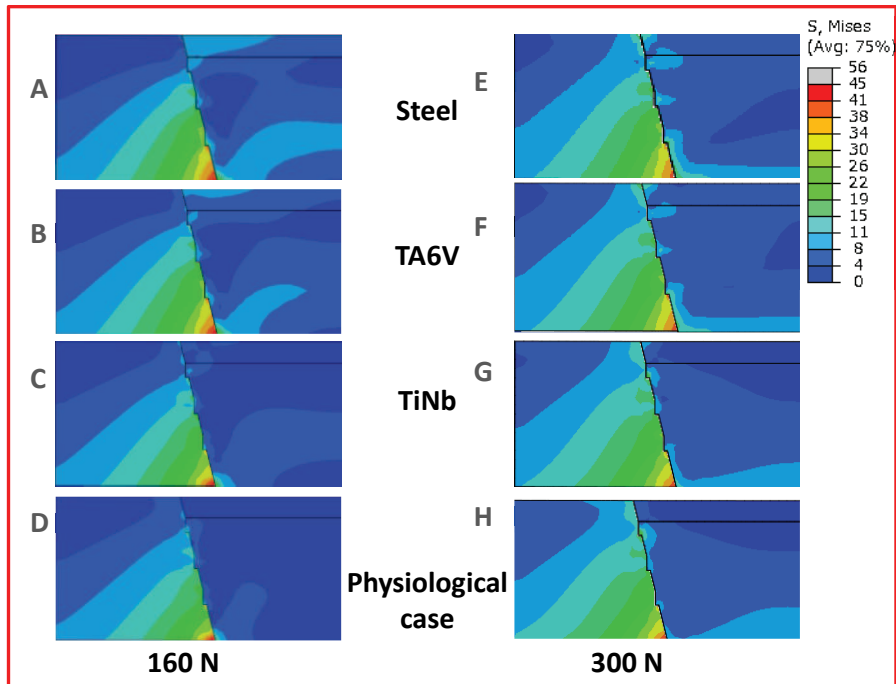
Fig. 9 - Representation of Von Mises stress in the implant and in the cortical bone in the S-MODEL for an axial load of 160 N applied on a smooth implant. Four Young's moduli of the implant are considered: a) Steel; b) TA6V; c) TiNb; d) R_C
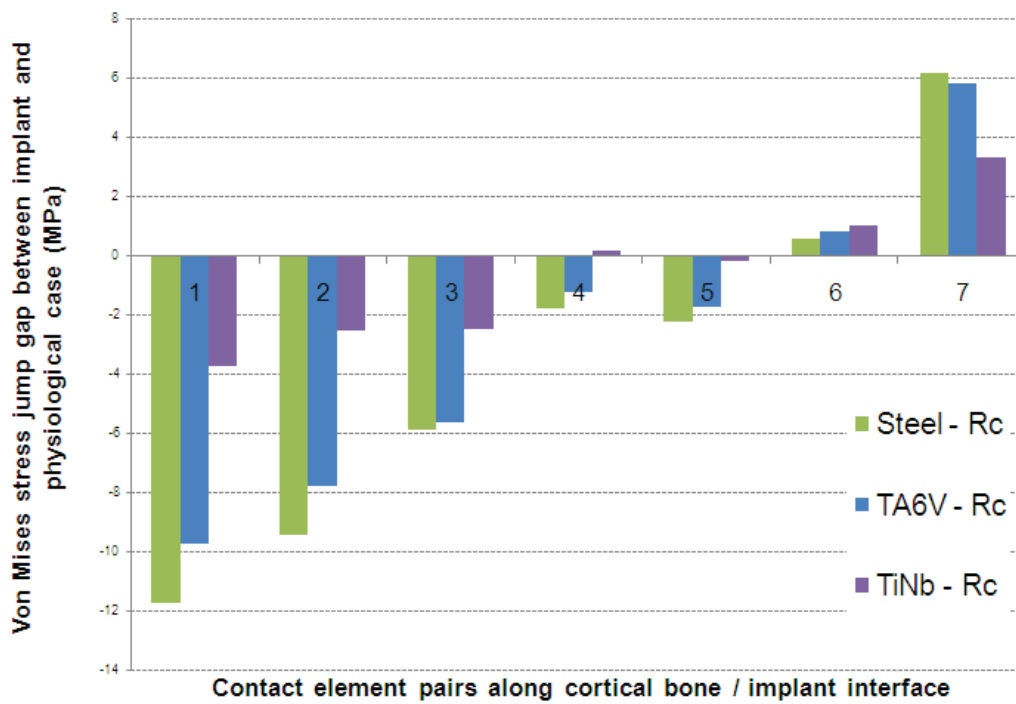
Fig. 10 - Representation of Von Mises stress jump between cortical bone and implant for an axial load of 160 N in the S-MODEL: gap between the implanted cases and the R_C. Three Young's moduli of the implant are considered: Steel - R_C ; TA6V - R_C ; TiNb - R_C

Fig. 11 - T-Model Von Mises stress distribution in the threaded implant and the cortical bone for axial loads of 160 N (A - Steel, B - TA6V, C - TiNb, D - R_C) and 300 N (E - Steel, F - TA6V, G -TiNb, H - R_C)
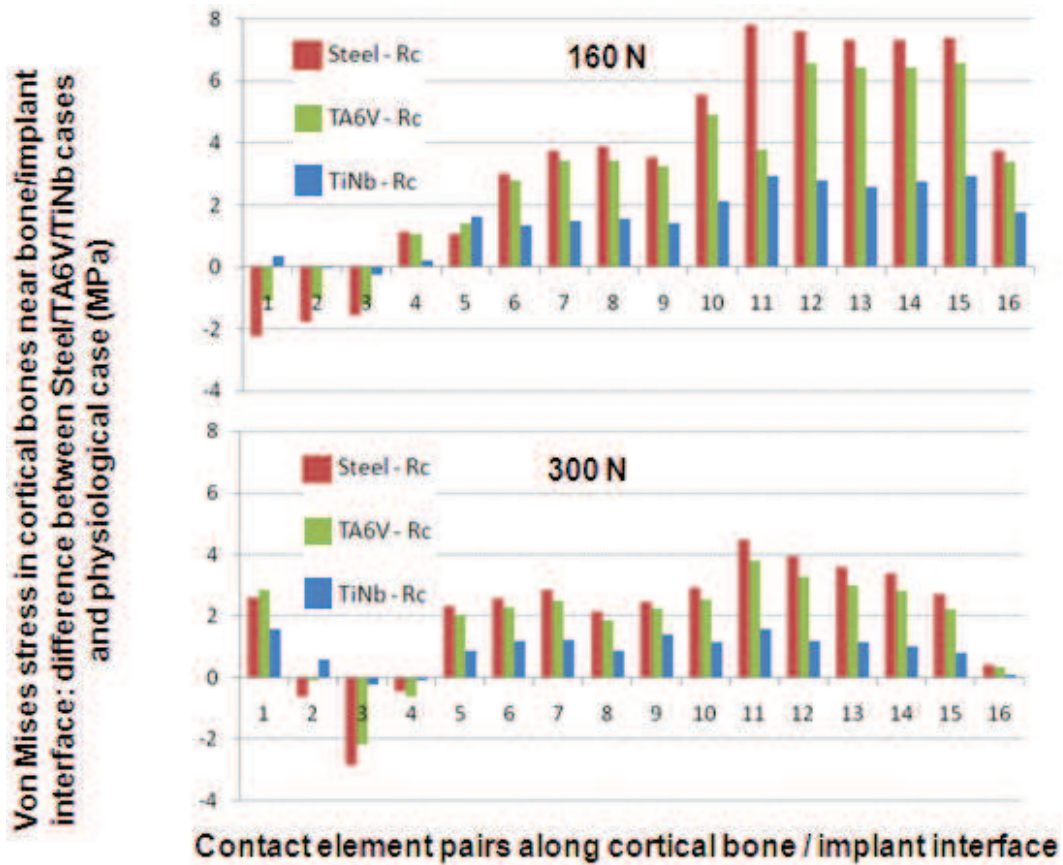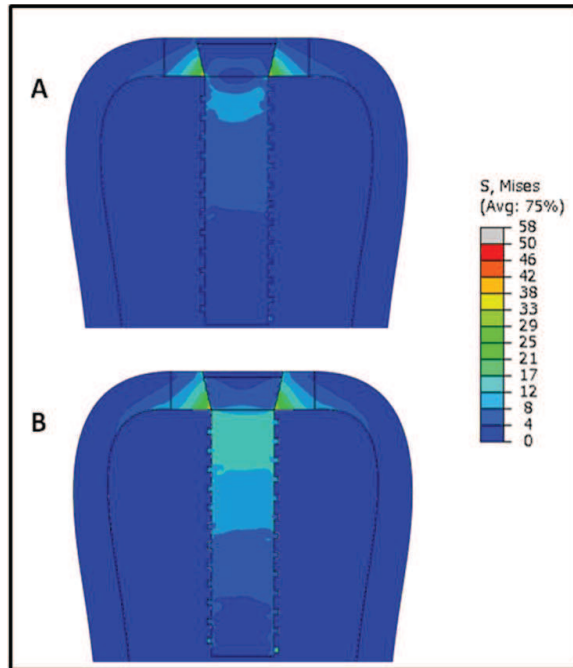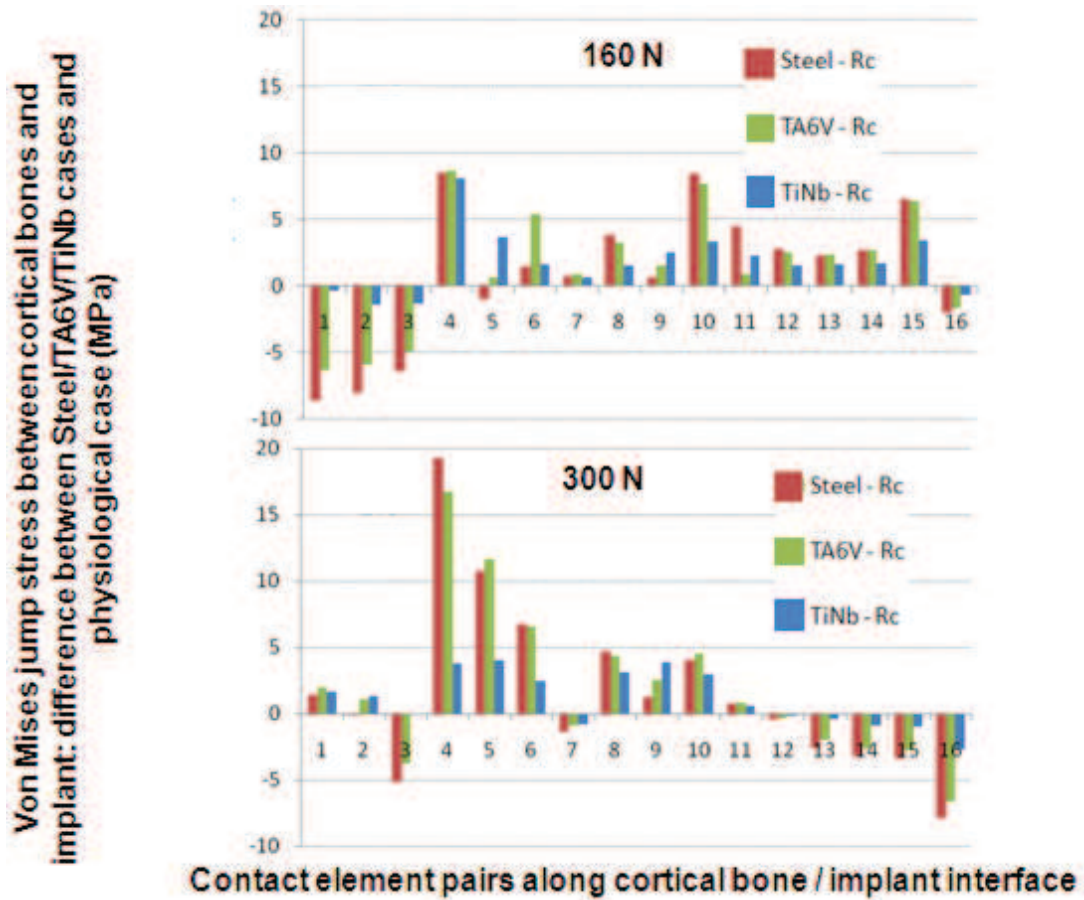
Fig. 12 - Representation of Von Mises stress gap in the cortical bone compared with R_C for an axial load of 160 N (top) and 300 N (bottom) applied on a threaded implant. Three Young's moduli of the implant are considered: Steel - R_C ; TA6V - R_C ; TiNb - R_C

Fig. 13 - Representation of Von Mises stress distribution in the considered system for loads of 160 N (A) and 300 N (B) in the case of TiNb implant

Fig. 14 - Representation of Von Mises stress jump between the cortical bone and the implant under an axial load of 160 N (up) and 300 N (down) applied on a threaded implant: gap between implanted case and R_C. Three Young's moduli of the implant are considered: Steel - R_C ; TA6V - R_C ; TiNb - R_C

Contact element pairs along cortical bone / implant interface
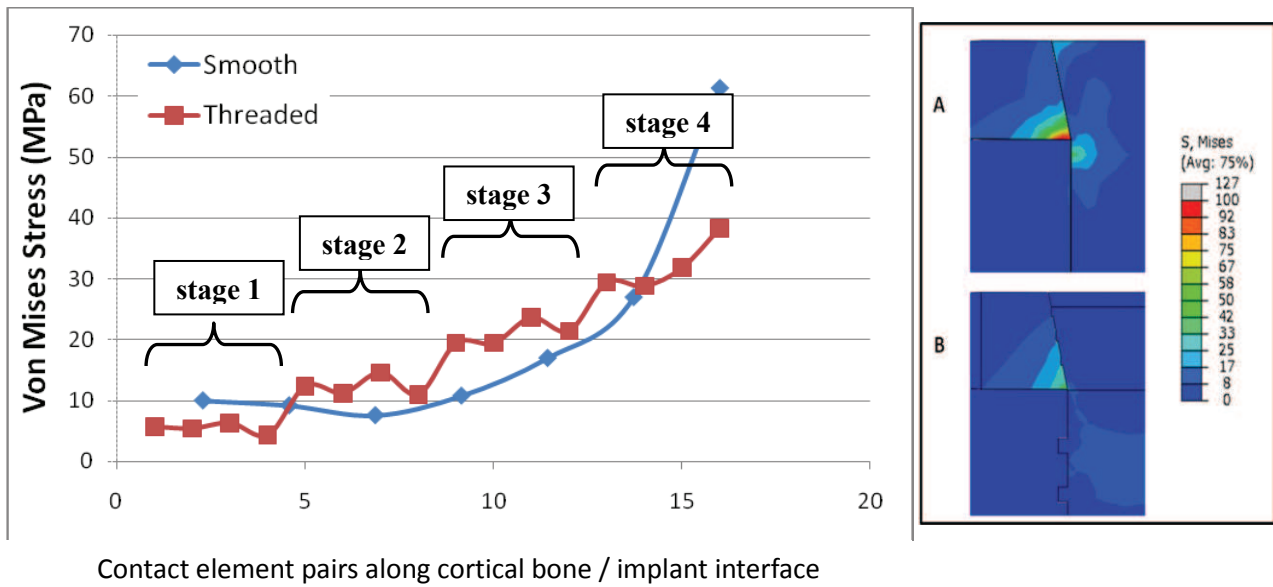
Fig. 15 - Von Mises stress distribution in TiNb implant and cortical bone under a load of 160 N: comparison between the S-MODEL (A) and the T-MODEL (B). On the left: Von Mises stress in the cortical bone near bone/implant contact surface – Four stage levels are clearly identified in the T-MODEL. On the right: comparison of stress distribution in various parts of the considered system